An analytical model for the celestial distribution of polarized light, accounting for polarization singularities, wavelength and atmospheric turbidity

Xin Wang[1,2], Jun Gao[1], Zhiguo Fan[1], Nicholas W. Roberts[2]

1. School of Computer and Information, Hefei University of Technology, No.193, Tunxi Road, Hefei, Anhui, China.
2. School of Biological Sciences, University of Bristol, Tyndall Avenue, Bristol, BS8 1TQ, UK.

Abstract

We present a computationally inexpensive analytical model for simulating celestial polarization patterns in variable conditions. We combine both the singularity theory of Dennis and Berry [1] and the intensity model of Perez [2] such that our single model describes 3 key sets of data: 1) The overhead distribution of the degree of polarization as well as the existence of neutral points in the sky; 2) the change in sky polarization as a function of the turbidity of the atmosphere; and 3) sky polarization patterns as a function of wavelength, calculated in this work from the ultra-violet (UV) to the near infra-red (IR). To verify the performance of our model we generate accurate reference data using a numerical radiative transfer model and statistical comparisons between these two methods demonstrate no significant difference in almost all situations. The development of our analytical model provides a novel method for efficiently calculating the overhead skylight polarization pattern. This provides a new tool of particular relevance for our understanding of animals that use the celestial polarization pattern as a source of visual information.

Keywords: sunlight; scattering; neutral points; radiative transfer; navigation.

1. Introduction

Light from the sun is unpolarized before it enters the Earth's atmosphere. However, as a result of elastic scattering events, primarily Rayleigh scattering in the transmission path, the light from the sky as it appears from the Earth is partially polarized. To a first approximation the structure of the polarization field in the sky is a principal function of the position of sun, where the angle of polarization is arranged along concentric circles around the sun's position [3]. This skylight polarization pattern is important in several contexts, but particularly as a principal source of navigational information to many different animals. With analogies to the use of a sun compass, insects such as bees [4], desert ants [5], locusts [6] and beetles [7] use the polarization pattern of the sky as a primary sensory cue for spatial orientation during seasonal migration or foraging journeys.

Over the last 30 years, attempts have been made to simulate the skylight polarization pattern. Being able to calculate the overhead polarization pattern has become important for several reasons, particular with regard to understanding the information available to animals and to the development of bio-inspired technologies. Our understanding of the basic physical process that creates the polarization pattern has resulted in the development of two main categories of model, both with varying levels of success. The first type of model is based on solving the vector radiative transfer equation (VRTE) through the Earth's atmosphere. Matrix operator theory [8], discrete ordinate theory [9], spherical harmonics theory [10] and multiple scattering theory [11] have all been applied to this numerical approach. Such modeling of the transmission processes requires detailed information about atmospheric composition, structure, and dynamics and whilst inherently accurate for the parameters modeled, the process is extremely computationally expensive and subject to the accuracy of the initial conditions. The alternate type of model is derived from characteristics of the skylight distribution and provides a set of analytic solutions to overhead polarization pattern. Existing models such as the Rayleigh single scattering model [3], the singularity theory model proposed by Dennis and Berry [1], or the analytical model developed by Wilkie [12] are not as accurate as solving vector radiative transfer

equations, however they achieve an acceptable tradeoff between the speed of computation and accuracy of describing broad scale features. To date, we still lack a complete analytic model that provides an accurate calculation of the overhead polarization as a function of wavelength, intensity, and atmospheric turbidity conditions.

The most commonly used model to calculate the angle of skylight polarization is the model based on Rayleigh single-scattering theory [13]. However, the properties of the simulated theoretical pattern differ considerably in terms of the angle of polarization and degree from the real sky [14-18] and bear little resemblance to the information available to animals [19-21]. In the single-scattering Rayleigh model, skylight intensity is considered to be a constant value across the sky, and the degree of polarization (DoP) is approximated to be dependent only on the scattering angle [3, 22]. To address where the simple Rayleigh model falls short, several studies have tried combining the Rayleigh scattering model and other atmospheric models. Nishita *et al.* (1996) first introduced a wavelength dependence for calculating the colour information of the sky based on a model of multiple scattering [23] and in 1999, Preetham *et al*. [24] also constructed a model to include wavelength information based on the widely used luminance model from Perez *et al.* [2]. Currently, the most advanced models that analytically predict the sky colour can be attributed to Haber *et al.* (2005) [25] who developed a physically based model following the same basic principle as Nishita et al. and a model by Hosek and Wilkie (2012) who built a full spectral sky model using Bezier curves [26]. Wilkie *et al.* (2004) also created a separate analytical sky model that makes the connection between polarization and skylight intensity [12].

Furthermore, the single-scattering Rayleigh model does not predict the four sky neutral points. In recent years, clear experimental evidence for the existence of four un-polarized points in the sky has been provided: 1) above the Sun (the Babinet point); 2) below the Sun (the Brewster point); 3) above the anti-Sun (the Arago point); and 4) below the anti-Sun (the second Brewster point) [27-30] and only the theory of Dennis and Berry [1] provides a satisfactory theoretical understanding.

Dennis and Berry [1] considered the sun and anti-sun points to be polarization singularities, each with index +1. Due to the instability of singularities with index +1, they each divide into two further singularities with index of +1/2 along the solar meridian (the line connecting the Sun to the zenith). The analytical model they proposed gave a more accurate description of the sky polarization pattern compared to the Rayleigh model, and reproduces not only the positions with zero DoP but also subtle variations in the polarization maxima. Their singularity model further agreed well with numerical multiple-scattering calculations and experimentally observed data.

In an attempt to advance our ability to efficiently and accurately calculate the skylight polarization pattern, we present in this work a new analytical model that focuses on the DoP (although the polarization angle can also be easily calculated), and includes the skylight intensity, wavelength and positions of neutral points in the sky. Our aim here is not to provide a new fundamental theory of how the polarization pattern is created, but to create a useful tool to generate a more exact representation of the celestial polarization pattern. The benefits of such a tool are envisaged to be three-fold. Firstly, it will provide a more convenient set of input parameters for future modeling and investigations of polarization information processing by insects and analogous bio-principled navigation systems. Secondly, it provides a convenient method for creating a representation of the overhead polarization pattern for behavioural studies using modified LCD polarization monitors [31-34]. Finally it is also applicable to furthering our understanding of multi areas of technology: for example remote sensing, autonomous navigation or metrology.

2. Theory

2.1 Combination of Polarization and Skylight Intensity

The polarization pattern model as an expression describes the relative DoP at any given point in the sky depending on the position of the sun.

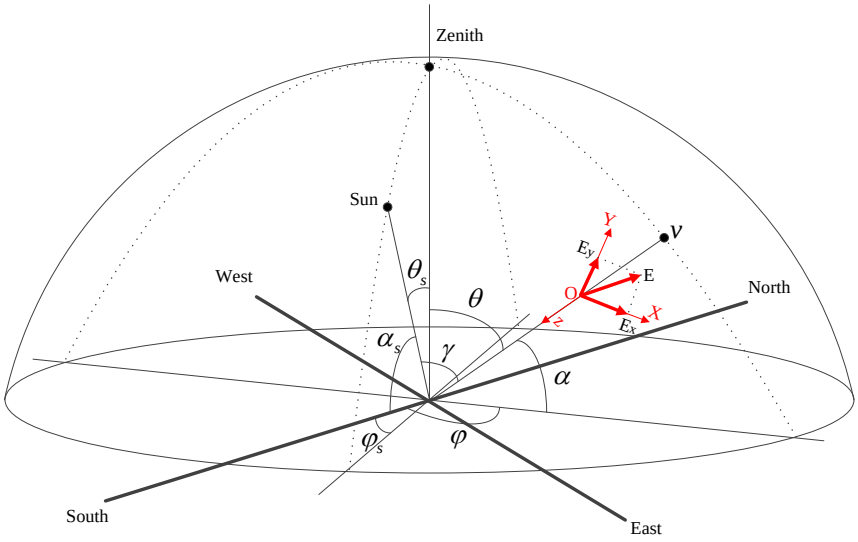

Figure 1: The coordinate for specifying the solar position and the viewing direction v in the sky. θ_s, α_s and φ_s are the zenith angle, elevation angle and azimuth angle of the sun respectively; θ, α and φ are the same angles for the viewing point; and γ is the scattering angle. When polarized light propagates on viewing direction v (z-axis), the electric field of the light vibrates in the perpendicular plane XOY (E_x and E_y represents the components of the electric field on x-axis and y-axis respectively). Image adapted after [24].

To describe the sky polarization pattern, we present viewing point v by Cartesian coordinates x,y or plane polar coordinates r,ϕ in the plane corresponding to the stereographic projection of v. The position of the viewing point could be defined using $\xi = x + iy = rexp(i\phi)$. In terms of field components within a Cartesian framework, polarization can be represented by a complex (un-normalized) Stokes parameter [35],

$$w(\xi) = \langle\left(E_x + iE_y\right)^2\rangle = \langle E_x^2\rangle - \langle E_y^2\rangle + 2i\langle E_x E_y\rangle = |w(\xi)|exp\{2i\psi(\xi)\}, \quad (1)$$

where the average is all scattered light arriving from position ξ. Then $|w(\xi)|$ is the DoP, $\psi(\xi)$ is the orientation of the polarization direction. According to Dennis and Berry [1], each individual polarization singularity, with index of +1/2, correspond to a $w(\xi) = 0$. In zenith-centered coordinates, if the sun moves on the y-axis, positions of neutral points would be

$$\xi_+ = i\frac{(y_s+L)}{(1-Ly_s)}, \xi_- = i\frac{(y_s-L)}{(1+Ly_s)}, -1/\xi_+^* , -1/\xi_-^* , \quad (2)$$

where y_s represents the y-coordinate of the sun. The angular separation of two adjacent neutral points is $\delta = 4\arctan(L)$, where L is a constant that used to describe the degeneracy of two singularities by defining $w(\xi)$ changes in proportion to the value of $-(\xi^2 + L^2)$. Here, ξ_+, ξ_- , $-1/\xi_+^*$ and $-1/\xi_-^*$ represent singularities below (Brewster) and above (Babinet) the sun, and above (Arago) and below (second Brewster) the anti-sun respectively. To set the DoP to be antipodally invariant we make $|w(-1/\xi^*)|$ equal to $|w(\xi)|$, such that the DoP is given by

$$w(\xi) = \frac{(\xi-\xi_+)(\xi-\xi_-)(\xi+1/\xi_+^*)(\xi+1/\xi_-^*)}{(1+r^2)^2|\xi_++1/\xi_+^*||\xi_-+1/\xi_-^*|} \quad (3)$$

From this point on we now extend the theory of Dennis and Berry [1] to include the azimuth of the sun, φ_s to allow the description of an arbitrary position for the sun. ξ_+ and ξ_- now become,

$$\xi_+ = \frac{x_s+Lcos(\varphi_s)}{1-Lcos(\varphi_s)x_s} + \frac{y_s+Lsin(\varphi_s)}{1-Lsin(\varphi_s)y_s}i, \quad (4)$$

$$\xi_- = \frac{x_s-Lcos(\varphi_s)}{1+Lcos(\varphi_s)x_s} + \frac{y_s-Lsin(\varphi_s)}{1+Lsin(\varphi_s)y_s}i, \quad (5)$$

where x_s represents the x-coordinate of the sun. We now add into the theory three further factors to account for 1) the effect different atmospheric conditions can have on the degree of polarization for scattered light 2) the greater than predicted depolarization that occurs near the horizon [3] 3) the fact that the DoP is a function of wavelength.

Firstly we take into account the effect different atmospheric turbidity conditions can have on the degree of polarization for scattered light. This modifies the DoP, to be

$$DoP(\xi, T) = |w(\xi)|M_{DoP}(T). \quad (6)$$

$M_{DoP}(T)$ influences the maximal of DoP in the sky, and we use the empirically determined formula proposed by Wilkie [12] to describe the gradual exponential fall off with rising of turbidity, T, as

$$M_{DoP}(T) = e^{-\frac{T}{k_1}+k_2}, \tag{7}$$

where the constants k_1 and k_2 are control parameters used to fit the relationship (k_1 and k_2 are set as 4 and 0.12 in our model).

Secondly, we describe the stronger depolarization effects near the horizon compared with the zenith by introducing a horizon correction factor, E, that has a maximum value at the zenith and decreases towards the horizon with the form,

$$E(\theta) = \cos(\theta)^{\frac{1}{N}}, \tag{8}$$

where N is a control parameter and set to 10 for our calculations [1].

Finally, to introduce into the model the dependence of the polarization on the wavelength of the sunlight, we adapt the model of Perez [2]. The original work by Perez [2] used a $CIE - XYZ$ colour space, however, whilst the parameter Y accurately describes the illumination, it proves a poor way to represent the X and Z variables [36]. Therefore we modify the representation to use the $CIE - Yxy$ color space as an alternative; this is a colour space that Preetham [24] showed to a better analytic representation. The chromaticity values x and y are related to Perez's five original parameters by

$$Y = Y,$$

$$x = \frac{X}{X+Y+Z},$$

and

$$y = \frac{Y}{X+Y+Z}. \tag{9}$$

Chromaticity values x and y can be calculated from the luminance parameters as defined by Perez

$$x = x_z \frac{F(\theta,\gamma)}{F(0,\theta_s)} \tag{10}$$

and

$$y = y_z \frac{F(\theta,\gamma)}{F(0,\theta_s)}, \tag{11}$$

where x_z, y_z represent the zenith chromaticity values x and y respectively, and F is given by

$$F_{perez}(\theta,\gamma) = (1 + Ae^{B/cos\theta})(1 + Ce^{D\gamma} + Ecos^2\gamma). \tag{12}$$

Full derivations of the parameters used here can be found in the supplemental material (equations S1-S5).

Wyszecki and Stiles [37] further showed that the relative spectral radiant power $S_D(\lambda)$ can be obtained by a linear combination of mean spectral radiant power $S_0(\lambda)$ and first two Eigen vector functions $S_1(\lambda)$ and $S_2(\lambda)$,

$$S_D(\lambda) = S_0(\lambda) + M_1 S_1(\lambda) + M_2 S_2(\lambda), \tag{13}$$

where the values of $S_0(\lambda)$, $S_1(\lambda)$ and $S_2(\lambda)$ are found in appendix table 2 from Preetham et al [24] and the the parameters M_1 and M_2 depend on the chromaticity values x and y calculated from equations 10 and 11.

$$M_1 = \frac{-1.3515-1.7703x+5.9114y}{0.0241+0.2562x-0.7341y}, \quad (14)$$

$$M_2 = \frac{0.0300-31.4424x+30.0717y}{0.0241+0.2562x-0.7341y}. \quad (15)$$

Substituting equation 13 into the model of Perez [12], the influence of spectral radiant power becomes

$$S(\gamma,\theta,\lambda) = \left(\frac{1}{S_D(\lambda)} - \frac{1}{S_{sun}(\lambda)}\right)\frac{S_{90}(\lambda)S_{sun}(\lambda)}{S_{sun}(\lambda)-S_{90}(\lambda)}, \quad (16)$$

where $S_{90}(\lambda)$ and $S_{sun}(\lambda)$ were the spectral radiant power values at 90° from the sun and for looking directly at the sun respectively.

Therefore, the combination of both the spectral dependence and correction for depolarization effect close to the horizon weighted accordingly results in the DoP becoming

$$DoP(\xi,\gamma,\theta,T,\lambda) = |w(\xi)|\left(\theta E(\theta) + \left(\frac{\pi}{2}-\theta\right)S(\gamma,\theta,\lambda)\right)M_{DoP}(T). \quad (17)$$

2.2 Stereographic Projections

The sky polarization pattern calculated using this model results in a 3-dimensional representation of the celestial DoP. In order to accurately display the results in the 2-dimensioanl plots presented in the results section, the calculated DoP values must be stereographically transformed to a 2-dimensional plane.

Fig. 2 illustrates the one-to-one correspondence between the points on the surface of the celestial hemi-sphere and the points in the projected plane [38]. The simple coordinate transformation between 3-D and 2-D projections is given by

$$x_m + iy_m = 2rtan(\theta/2)\exp(i\varphi). \quad (18)$$

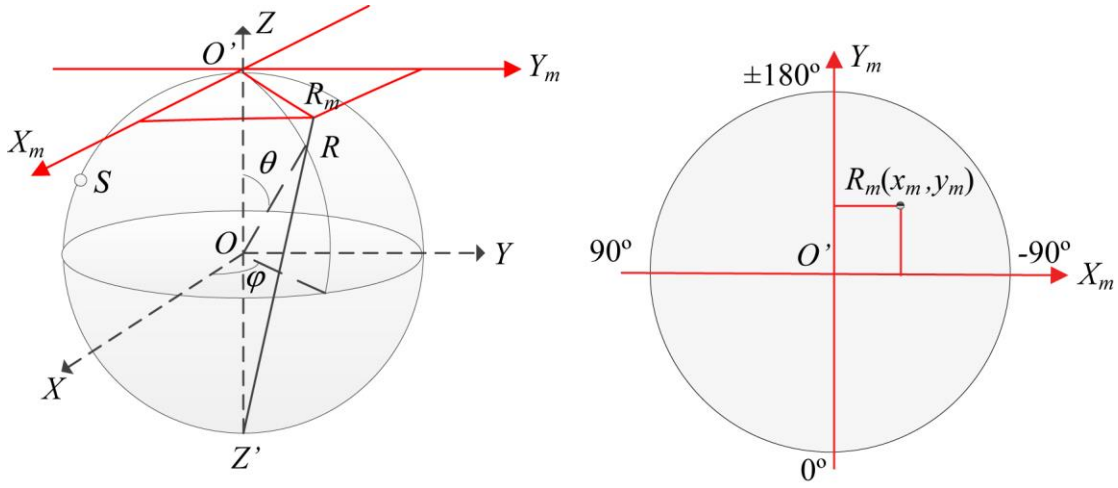

Figure 2: Schematic diagram for the stereographic projection from 3D to 2D. The left picture is the coordinate used in 3D space, and the right picture is the coordinate used in 2D space.

2.3 Reference Data Generation

Obtaining an accurate data set of actual polarization sky pattern for comparison with our model presents something of a challenge. To the best of our knowledge, no experimentally measured dataset of the skylight polarization pattern currently exists for a variety of wavelengths, sky turbidities and with sufficient spatial resolution to illustrate the neutral points. Whilst testing our model against experimental data would be the most preferable situation, we have therefore had to take a different approach. We used a standard numerical method [26, 39, 40], where the overhead polarization pattern was calculated via a numerical simulation of atmospheric light transformation and employed the widely used open source software Libradtran [41] as our reference data generator. The Libradtran software package is a suite of tools for radiative transfer calculations in the Earth's atmosphere. It can be used to compute solar radiance, irradiance and energy fluxes in both the solar and terrestrial part of the spectrum with specified parameters including position of the sun, components of the air, polarization, turbidity and wavelength as required [41, 42]. The simulation program was written using Python and run on Mac OS 10.10. It should be noted that

comparative calculations took approximately 4000 times longer than our analytic method.

Version 1.7 of the Libradtran was used in all of our simulations; utilizing the radiative transfer equation solver (RTE_SOLVER), set as MYSTIC and with the MC_POLARISATION option turned on. The number of photons (MC_PHOTONS) was set as 100000; surface albedo (ALBEDO) was set as zero; solar azimuth angle (PHI0) was set as 30; aerosol season (AEROSOL_SEASON) was set as spring-summer profile. To simulate different sun elevation situations, solar zenith angles (SZA) were set as 25, 65 and 85; to simulate different turbidity conditions, horizontal visibilities in km (AEROSOL_VISIBILITY) were set as 16, 8 and 4, while the wavelength dependence of aerosol optical depth (AEROSOL_ANGSTROM) was set to (1.3, 0.0463), (1.3, 0.1385) and (1.3, 0.3228) as AEROSOL_ANGSTROM was used to scale the aerosol optical depth using the Angstrom [43] formula $\tau = \beta\lambda^{-\alpha}$ (here, $\alpha = 1.3$ and $\beta = [0.0463, 0.1385, 0.3228]$); to simulate the performances of different wavelengths, wavelengths (WAVELENGTH) were set as 380, 450, 500, 550, 600, 650, 700 and 780 respectively.

3. Results and Discussion

3.1 Simulation Results of Sky Polarization Pattern Model

Figure 3 is a representative sample of the analytic results from our model for systematic variations in solar azimuth, solar elevation, atmospheric turbidity, and wavelength. Contour plots of varying azimuth angle clearly depict the positions of neutral points (fig 3a). The two open circles above and below the sun are the Babinet and Brewster points respectively. The Argo point (above the anti-sun) can also be seen in when the sun is located close to the horizon (fig 3c, leftmost panel).

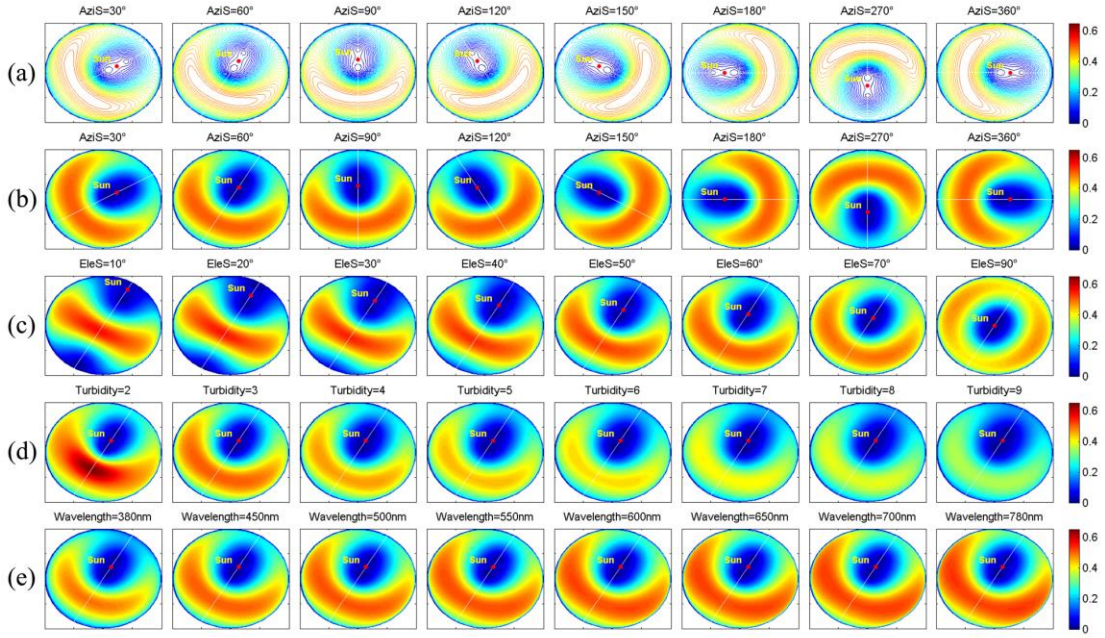

Figure 3: Simulation results of sky polarization pattern. A different set of parameters is varied for each row of panels as follows: (a) and (b) - solar azimuth angle (Axis; (a) = contour plot; (b) = heat-map); (c) solar elevation (EleS); (d) turbidity; and (e) wavelength. Colour hues indicate the degree of polarization (DoP). Unless being varied, parameters were maintained at the following values for all plots: turbidity (T) = 3, wavelength = 450 nm, solar elevation = 60°, and azimuth angle = 60°.

Increasing the value of the sky turbidity results in a decrease in DoP, as expected (fig 3d). Finally, as wavelength is changed from 380nm to 780nm corresponding changes in DoP are observed (fig 3e), matching the previous findings of Aben [44] and Lee [45].

3.2 Comparison with numerical radiative transfer model

To investigate the validity of our new model we compared our results to the accepted standard radiative transfer model [46-48]. Three different solar elevation angles (5°, 25°, 65°) and three different turbidity conditions (2, 4, 8) were selected to facilitate nine groups of comparisons between the analytic results of our model and those of the Libradtran [41, 42] numerical solutions. Figure 4 illustrates the comparison between three groups of calculations all with a turbidity of 2 (figures in S1 and S2 of supplementary material show the situations of turbidity 4 and 8 respectively). We see that the simulation results of our model closely approximate the reference data. However, one principal area of difference exists at the regions with lower degrees of

polarization (deep blue regions in figure 4, S1 and S2). Here, the DoP values predicted by our model were lower than those of the reference data, especially for situations with larger solar elevation angles (fig 4c). Overall however, we find no overall statistically significant differences between our model and the numerical simulation (Table 1, supplementary information) and we should note again the slow speed of the numerical calculations makes Libradtran impractical to be used in many situations.

3.3 Comparison with the single-scattering Rayleigh model and the model proposed by Wilkie

We further investigated the comparative accuracy of two of the other commonly used models: the single-scattering Rayleigh model [3] and the model proposed by Wilkie [12]). In all cases we chose five different initial parameter sets for the comparisons (Fig 5). In the same way as for Fig. 3, the first two rows of Fig. 5 illustrate our model in the form of a contour plot of isolines for the DoP and a false colour surface plot. The results of the single-scattering Rayleigh model are shown in the third row of Fig. 5 and show an accurate representation of spatial structure of DoP for the majority of the sky. However, the calculation returns a poor depiction of the absolute values of the DoP, with accuracy deteriorating at angles further for the solar elevation. Moreover, the neutral points are not predicted. The model proposed by Wilkie (fourth line of figure 5) that combines the single-scattering Rayleigh model with the skylight intensity fails to describe accurately, both the spatial form of the DoP and the positions of the neutral points in the sky. Note the scale bar changes for Fig. 5(a-e)

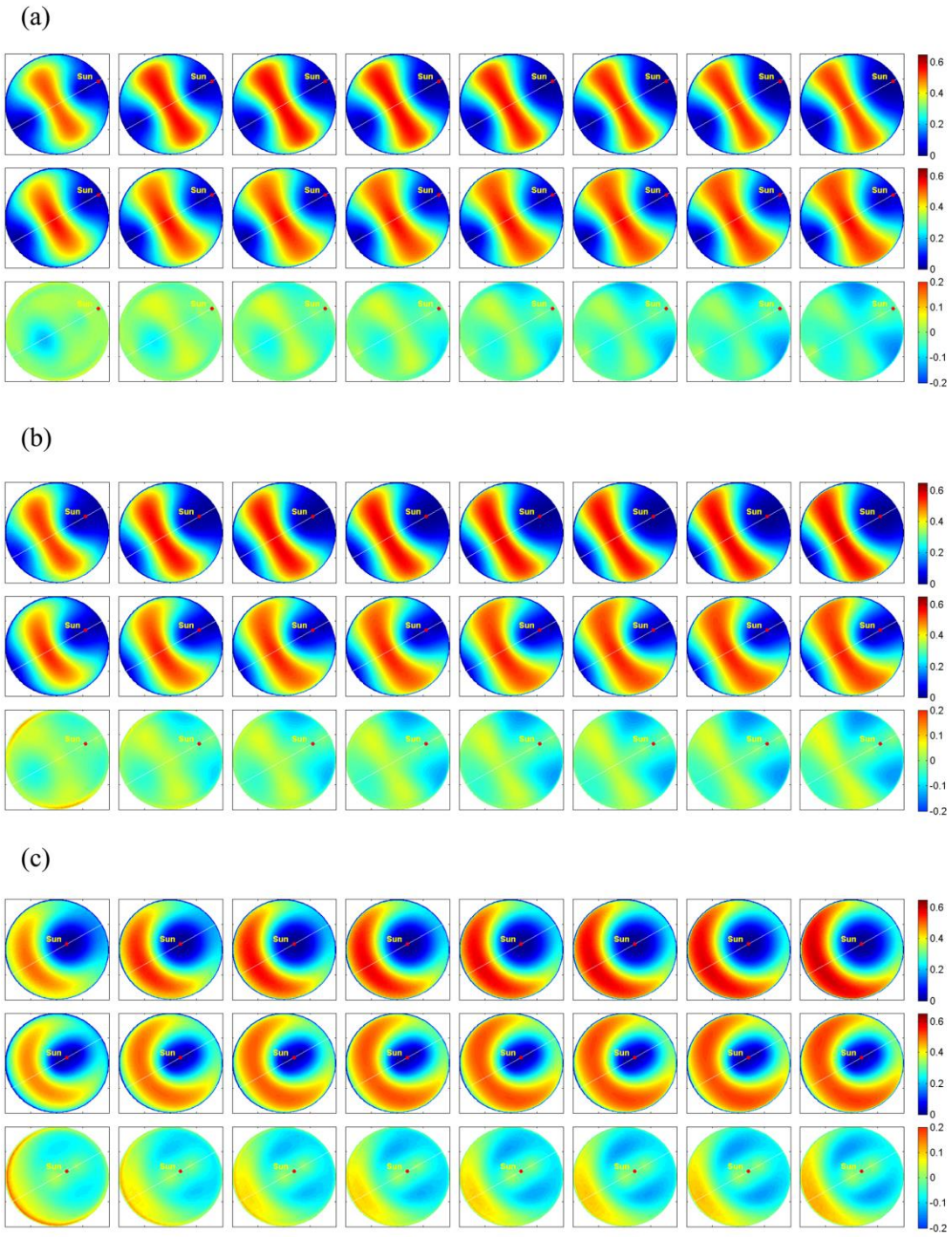

Figure 4: Comparison between our model and the Libradtran. All the simulations were implemented with a solar azimuth angle of 30° and a turbidity of 2. Solar elevation angles were (a) 5°, (b) 25° and (c) 65° respectively. Within each section, row 1 = Libradtran simulation; row 2 = our model output; and row 3 = relative differences between row 1 and 2. Columns represent comparisons under eight different wavelength conditions (380nm, 450nm, 500nm, 550nm, 600nm, 650nm, 700nm and 780nm, respectively). Heat map colours indicate the degree of polarization; 'AziS' - solar azimuth angle; 'EleS' - the solar elevation angle, and the red point illustrates the position of the sun.

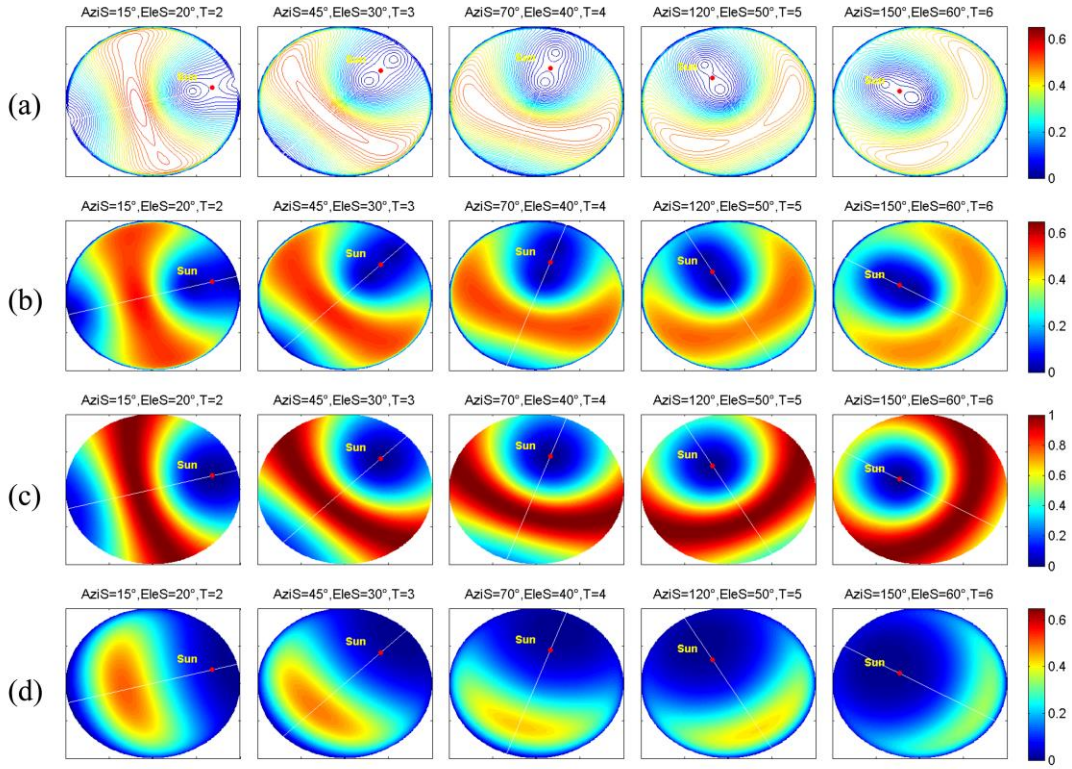

Figure 5: Comparisons between (a-b) our model, (c) the single-scattering Rayleigh model, and (d) the model proposed by Wilkie. The simulation results are presented in five different situations (each of the 5 columns) in which (from left to right) turbidity increases from 2 to 6, solar azimuth (AziS) increases from 15° to 150°, and solar elevation (EleS) increases from 20° to 60°. Hue indicates the degree of polarization and the red point illustrates the position of the sun.

4. Conclusions

In this paper, we have presented an efficient and accurate analytical model of the sky polarization pattern. The model is based on the singularity theory, and therefore illustrates the existence of neutral points in the sky. To reiterate an important point made originally by Berry and Dennis [1], the comparisons between our new model and the reference data illustrate how the broad scale patterns across the whole sky intrinsically depend on the form of local singularities. Our model provides an important advance by demonstrating how the distribution of the degree of polarization the skylight changes according to the given parameters of solar position, turbidity condition and skylight wavelength. The performance of our model was verified

against a numerical simulation of atmospheric light transport (using Libradtran [41, 42]) and no significant difference was found between them in most situations. Due to the great number of parameters that can be included in our model it is slightly more computationally costly than the single-scattering Rayleigh model, however it is still very efficient when compared with any radiative transfer simulation, such as Libradtran, and results in a considerable increase in accuracy over existing models.

Our future efforts will concentrate on enhancing the accuracy of our model. The differences between our model and the numerical simulations currently occur in the regions with low degree of polarization near the sun and near the horizon and this warrants further investigation into understanding the physical reasons for this. As a computationally inexpensive analytical model, the optical effects of different types of aerosols have not yet been included, though the shape, size and material configurations of aerosols do have considerable influences on the shape of scattering phase function [49, 50] being particular to different atmospheric conditions. In addition, the distance between neutral points in our model was also seen to be constant under all sky conditions, whereas experimental observations [51-53] have demonstrated that the locations of these points do change according to the turbidity condition in the sky.

Finally, we envisage that this new tool will provide a useful method for generating physiologically relevant polarization patterns for use in future behavioural studies. Recent advances in the creation of dynamic polarization stimuli [31, 32, 54, 55] have the potential to use this model for the controllable presentation of celestial polarization behavioural cues. The efficient generation of polarization patterns provides a novel paradigm for future investigations into the limits of polarization orientation behaviour and how the fusion of multi modal signals can be dynamically tuned [56].

5. Acknowledgments

The authors would like to thank the Air Force Office of Scientific Research (grant # FA8655-12-2112), National Science Foundation of China (grant # 61571175) and the Chinese Science Council Scholarship scheme.

6. References

[1] Berry M V, Dennis M R, Lee Jr R L. Polarization singularities in the clear sky [J]. New Journal of Physics, 2004, 6(1): 162.

[2] Perez R, Seals R, Michalsky J. All-weather model for sky luminance distribution-preliminary configuration and validation [J]. Solar energy, 1993, 50(3): 235-245.

[3] Coulson K L. Polarization and Intensity of Light in the Atmosphere [M]. A Deepak Pub, 1988.

[4] Labhart T. Specialized photoreceptors at the dorsal rim of the honeybee's compound eye: polarizational and angular sensitivity [J]. Journal of comparative physiology, 1980, 141(1): 19-30.

[5] Duelli P, Wehner R. The spectral sensitivity of polarized light orientation inCataglyphis bicolor (Formicidae, Hymenoptera) [J]. Journal of comparative physiology, 1973, 86(1): 37-53.

[6] Heinze S, Homberg U. Maplike representation of celestial E-vector orientations in the brain of an insect [J]. Science, 2007, 315(5814): 995-997.

[7] Dacke M, Nordström P, Scholtz C, et al. A specialized dorsal rim area for polarized light detection in the compound eye of the scarab beetle Pachysoma striatum [J]. Journal of Comparative Physiology A, 2002, 188(3): 211-216.

[8] Plass G N, Kattawar G W, Catchings F E. Matrix operator theory of radiative transfer. 1: Rayleigh scattering [J]. Applied Optics, 1973, 12(2): 314-329.

[9] Stamnes K, Conklin P. A new multi-layer discrete ordinate approach to radiative transfer in vertically inhomogeneous atmospheres [J]. Journal of Quantitative Spectroscopy and Radiative Transfer, 1984, 31(3): 273-282.

[10] Karp A H, Greenstadt J, Fillmore J A. Radiative transfer through an arbitrarily thick, scattering atmosphere [J]. Journal of Quantitative Spectroscopy and Radiative Transfer, 1980, 24(5): 391-406.

[11] Irvine W M. Multiple scattering in planetary atmospheres [J]. Icarus, 1975, 25(2): 175-204.

[12] Wilkie A, Ulbricht C, Tobler R F, et al. An analytical model for skylight polarisation [C]//Rendering Techniques. 2004: 387-398.

[13] Rayleigh L. XXXIV. On the transmission of light through an atmosphere containing small particles in suspension, and on the origin of the blue of the sky [J]. The London, Edinburgh, and Dublin Philosophical Magazine and Journal of Science, 1899, 47(287): 375-384.

[14] Suhai B, Horváth G. How well does the Rayleigh model describe the E-vector distribution of skylight in clear and cloudy conditions? A full-sky polarimetric study [J]. JOSA A, 2004, 21(9): 1669-1676.

[15] Pomozi I, Horváth G, Wehner R. How the clear-sky angle of polarization pattern continues underneath clouds: full-sky measurements and implications for animal orientation [J]. Journal of Experimental Biology, 2001, 204(17): 2933-2942.

[16] Emde C, Buras R, Mayer B, et al. The impact of aerosols on polarized sky radiance: model development, validation, and applications [J]. Atmospheric Chemistry and Physics, 2010, 10(2): 383-396.

[17] Pust N J, Shaw J A. Digital all-sky polarization imaging of partly cloudy skies [J]. Applied optics, 2008, 47(34): H190-H198.

[18] Horváth G. Polarized light and polarization vision in animal sciences [M]. Springer Berlin Heidelberg, 2014.

[19] Roberts N W, Porter M L, Cronin T W. The molecular basis of mechanisms underlying polarization vision [J]. Philosophical Transactions of the Royal Society B: Biological Sciences, 2011, 366(1565): 627-637.

[20] Wehner R. Polarization vision–a uniform sensory capacity? [J]. Journal of Experimental Biology, 2001, 204(14): 2589-2596.

[21] el Jundi B, Pfeiffer K, Heinze S, et al. Integration of polarization and chromatic cues in the insect sky compass [J]. Journal of Comparative Physiology A, 2014, 200(6): 575-589.

[22] Ebert D S. Texturing & modeling: a procedural approach [M]. Morgan Kaufmann, 2003.

[23] Nishita T, Dobashi Y, Nakamae E. Display of clouds taking into account multiple anisotropic scattering and sky light [C]//Proceedings of the 23rd annual conference on Computer graphics and interactive techniques. ACM, 1996: 379-386.

[24] Preetham A J, Shirley P, Smits B. A practical analytic model for daylight [C]//Proceedings of the 26th annual conference on Computer graphics and interactive techniques. ACM

Press/Addison-Wesley Publishing Co., 1999: 91-100.

[25] Haber J, Magnor M, Seidel H P. Physically-based simulation of twilight phenomena [J]. ACM Transactions on Graphics (TOG), 2005, 24(4): 1353-1373.

[26] Hosek L, Wilkie A. An analytic model for full spectral sky-dome radiance [J]. ACM Transactions on Graphics (TOG), 2012, 31(4): 95.

[27] Horváth G, Gál J, Pomozi I, et al. Polarization portrait of the Arago point: video-polarimetric imaging of the neutral points of skylight polarization [J]. Naturwissenschaften, 1998, 85(7): 333-339.

[28] Brewster D. XXL.—Observations on the Polarisation of the Atmosphere, made at St Andrews in 1841, 1842, 1843, 1844, and 1845 [J]. Transactions of the Royal Society of Edinburgh, 1863, 23(02): 211-239.

[29] Horváth G, Bernáth B, Suhai B, et al. First observation of the fourth neutral polarization point in the atmosphere [J]. JOSA A, 2002, 19(10): 2085-2099.

[30] Gál J, Horváth G, Meyer-Rochow V B, et al. Polarization patterns of the summer sky and its neutral points measured by full–sky imaging polarimetry in Finnish Lapland north of the Arctic Circle [C]//Proceedings of the Royal Society of London A: Mathematical, Physical and Engineering Sciences. The Royal Society, 2001, 457(2010): 1385-1399.

[31] Pignatelli V, Temple S E, Chiou T H, et al. Behavioural relevance of polarization sensitivity as a target detection mechanism in cephalopods and fishes [J]. Philosophical Transactions of the Royal Society B: Biological Sciences, 2011, 366(1565): 734-741.

[32] Temple S E, Pignatelli V, Cook T, et al. High-resolution polarisation vision in a cuttlefish [J]. Current Biology, 2012, 22(4): R121-R122.

[33] How M J, Pignatelli V, Temple S E, et al. High e-vector acuity in the polarisation vision system of the fiddler crab Uca vomeris [J]. The Journal of experimental biology, 2012, 215(12): 2128-2134.

[34] How M J, Marshall N J. Polarization distance: a framework for modelling object detection by polarization vision systems [J]. Proceedings of the Royal Society of London B: Biological Sciences, 2014, 281(1776): 20131632.

[35] Azzam R M A, Bashara N M. Ellipsometry and polarized light [M]. North-Holland. Sole

distributors for the USA and Canada, Elsevier Science Publishing Co., Inc., 1987.

[36] Lee R L. Digital imaging of clear-sky polarization [J]. Applied optics, 1998, 37(9): 1465-1476.

[37] Wyszecki G, Stiles W S. Color science [M]. New York: Wiley, 1982.

[38] Dietz R, Hoschek J, Jüttler B. An algebraic approach to curves and surfaces on the sphere and on other quadrics [J]. Computer Aided Geometric Design, 1993, 10(3): 211-229.

[39] Davis A B, Garay M J, Xu F, et al. 3D radiative transfer effects in multi-angle/multispectral radio-polarimetric signals from a mixture of clouds and aerosols viewed by a non-imaging sensor [C]//SPIE Optical Engineering+ Applications. International Society for Optics and Photonics, 2013: 887309-887309-18.

[40] Yang P, Bi L, Baum B A, et al. Spectrally consistent scattering, absorption, and polarization properties of atmospheric ice crystals at wavelengths from 0.2 to 100 μm [J]. Journal of the Atmospheric Sciences, 2013, 70(1): 330-347.

[41] Mayer B, Kylling A. Technical note: The libRadtran software package for radiative transfer calculations-description and examples of use [J]. Atmospheric Chemistry and Physics, 2005, 5(7): 1855-1877.

[42] Mayer B, Kylling A, Emde C, et al. libRadtran user's guide [J]. 2012.

[43] Angstrom A. On the atmospheric transmission of sun radiation and on dust in the air [J]. Geografiska Annaler, 1929, 11: 156-166.

[44] Aben I, Helderman F, Stam D M, et al. Spectral fine‐structure in the polarisation of skylight [J]. Geophysical research letters, 1999, 26(5): 591-594.

[45] Lee R L, Samudio O R. Spectral polarization of clear and hazy coastal skies [J]. Applied optics, 2012, 51(31): 7499-7508.

[46] Mayer B. Radiative transfer in the cloudy atmosphere [C]//EPJ Web of Conferences. EDP Sciences, 2009, 1: 75-99.

[47] Ota Y, Higurashi A, Nakajima T, et al. Matrix formulations of radiative transfer including the polarization effect in a coupled atmosphere–ocean system [J]. Journal of Quantitative Spectroscopy and Radiative Transfer, 2010, 111(6): 878-894.

[48] Cornet C, C-Labonnote L, Szczap F. Three-dimensional polarized Monte Carlo atmospheric

radiative transfer model (3DMCPOL): 3D effects on polarized visible reflectances of a cirrus cloud [J]. Journal of Quantitative Spectroscopy and Radiative Transfer, 2010, 111(1): 174-186.

[49] Kocifaj M, Gangl M, Kundracik F, et al. Simulation of the optical properties of single composite aerosols[J]. Journal of aerosol science, 2006, 37(12): 1683-1695.

[50] Kocifaj M, Kundracík F, Videen G. Optical properties of single mixed-phase aerosol particles[J]. Journal of Quantitative Spectroscopy and Radiative Transfer, 2008, 109(11): 2108-2123.

[51] Bellver C. Influence of particulate pollution on the position of neutral points in the sky at Seville (Spain) [J]. Atmospheric Environment (1967), 1987, 21(3): 699-702.

[52] Adams J T, Kattawar G W. Neutral points in an atmosphere-ocean system. 1: Upwelling light field [J]. Applied optics, 1997, 36(9): 1976-1986.

[53] Adams J T, Gray D J. Neutral points in an atmosphere-ocean system. 2: Downwelling light field [J]. Applied optics, 2011, 50(3): 335-346.

[54] How M J, Porter M L., Radford, A N., Feller, K D, Temple, S E, Caldwell, R L, Marshall, N J, Cronin, T W, Roberts, N W. Out of the blue: the evolution of horizontally polarized signals in *Haptosquilla* (Crustacea, Stomatopoda, Protosquillidae). Journal of Experimental Biology, 2014, 217: 3425-3431.

[55] How, M J, Christy, J, Roberts, N W, Marshall, N J. Null point of discrimination in crustacean polarisation vision. Journal of Experimental Biology, 2014 217:2462-2467.

[56] el Jundi, B, Warrant, E J, Byrne, M J, Khaldy, L, Baird, E, Smolka, J, Dacke, M. Neural coding underlying the cue preference for celestial orientation. Proceedings of the National Academy of Sciences, 2015, 112(36): 11395-11400.